Biophysical Chemistry 25 (1986) 43–55
Elsevier

BPC 01089

THE EFFECTS OF *n*-PENTANE ON VOLTAGE-CLAMPED SQUID NERVE SODIUM CURRENTS

A REINTERPRETATION USING KINETICS OF ORDERED SYSTEMS

Kenneth A. RUBINSON

* *The Five Oaks Research Institute, P.O. Box 507, Yellow Springs, OH 45387 and Department of Physiology and Biophysics, University of Cincinnati Medical Center, Cincinnati, OH 45267-0576, U.S.A.*

Received 6th December 1985
Revised manuscript received 29th May 1986
Accepted 15th July 1986

Key words: Voltage clamp; Sodium current; n-Pentane; Nerve conduction; Kinetics; Ordered system

The sodium-current voltage-clamp data of Haydon and Kimura obtained on squid nerves treated with *n*-pentane (J. Physiol. 312 (1981) 57) are fitted with a previously described model (K.A. Rubinson, J. Physiol. 281 (1978) 14P; Biophys. Chem. 15 (1982) 245). The apparently complex action of the perturbant can be interpreted as due to a shift in shielding of the applied potential jumps, a change in channel conductivity, and an increase in the rate constant of channel shutoff. The shift in shielding due to *n*-pentane is found to be quantitatively the same for variables describing both kinetic and equilibrium quantities, which are independent. The transmembrane sodium potential remains unchanged, however.

1. Introduction and background

Until recently the experiments probing the sodium channels of nerve primarily relied on voltage-clamping for the current-measuring assay. Patch-clamping and noise spectral measurements are being used increasingly since a wider range of tissues can be probed. In both cases, one aim is to understand – or at least limit the possible choices of – the kinetic and structural models to explain the time-dependent and voltage-dependent sodium currents.

In a simple clamp experiment the opening times of channels are distributed in time after the step-jump in potential. This behavior is clearly seen in patch-clamp noise-analysis experiments [1–4]. The distribution in opening times was originally designated by the author as 'heterogeneous kinetics' [5]. Subsequently, it has been found that analyses of this type have been done for numerous types of chemical reactions where the reactants retain at least some spatial order over the measurement time of the reaction. Included in these are fast solution reactions initiated by irradiation [6].

In analogy to these fast-reaction results, it was suggested that the opening-time distribution can result from a nonconcerted chemical process – simultaneous thermal and electrodiffusion of some part of the sodium channel – resulting in a conformational transformation of the channels [5,7]. Since the diffusing entity is likely to be bound within a macromolecular assembly, the motion is not diffusive in the usual sense of random free motion over an extensive time. Knapp et al. [8] use the term quasi-diffusive mode to describe motions of constrained submolecular units for which the motion cannot be discerned from conventional diffusion over the time course of the experimental

* Address for correspondence.

measurement. This quasi-diffusion proceeds over a distance of the order of 1 nm or less, and it cannot be observed in conventional ways that measure migration distances of 1 μm and larger. Nevertheless, the diffusion coefficient and viscosity associated with the quasi-diffusion over 0.1 ms and longer periods (the approximate time of the sodium channel kinetics) are expected to be of the same magnitude as for regular diffusion.

As pointed out in extensive detail by MacDonald [9], time lags can be modeled as concerted processes or distributed ones. He notes that the concerted processes represent deterministic models and the distributed lags represent stochastic models. The latter are expected [9]. This point of view previously had been extensively demonstrated in studies of the kinetics of reactions involving polymers. For instance, in relaxation measurements a distribution of relaxation times always appears. Peterlin [10] has presented a short, clear discussion of the origin of the heterogeneity in macromolecular translation. The theoretically more tractable and experimentally more accessible area of molecular rotation was treated generally by Cukier and Lakatos-Lindenberg [11]. They showed how the introduction of anisotropy into the molecular environment results in a distribution of relaxation times. This is abundantly observed at the atomic level in, e.g., ^{13}C-NMR. Heatley and Begum [12] describe a number of different treatments of the distribution of relaxation times found experimentally. One specific example is found in the relaxation of a protein sampled in the range 10^{-7}–10^{-9} s by Mössbauer emission. The temperature dependence of the lineshapes could only be fitted by assuming occupation of a distribution of conformations [8].

Thus, it would appear questionable whether the use of any small set of microscopic states describing the kinetics of biomacromolecular systems will lend much chemical insight (such as structure-function relationships) into the sodium channel or, perhaps, allosteric enzymes. A notable effort was made by Horn and Vandenberg [13] to test a large number of kinetic schemes on noise-analysis data from sodium channels. All but one (see ref. 14) other sodium channel kinetics model of which the author is aware are formulated using the concerted kinetics of small molecular assemblies as well. A recent review by Fishman [15] outlines the majority of models of the sodium channel kinetics.

The remainder of the paper is organized as follows. Section 2 contains a brief review of fundamental characteristics of the author's model. In section 3 is a presentation of some data consistent with the model which have subsequently appeared. Section 4 follows with the results of the data fitting on *n*-pentane-treated nerves and the associated controls. Finally, section 5 includes some suggested interpretations of the results. A companion paper [15a] presents a general discussion of interpretations (with continuum models) of the sodium channels' P_{open} voltage dependence. P_{open} data from both noise analyses and as derived here from clamp experiments are both included and are directly comparable.

In both papers, the term 'variable' is used for a quantity in the curve-fitting equation used to fit the experimental data. The variables include rate constants, delay times, and quantities used to scale the currents (e.g., mA or mA cm^{-2}). On the other hand, the term 'parameter' alludes to a quantity which appears in an equation describing relationships of the variables to, e.g., potential. The parameters include diffusion coefficients, charges of activation, conductances, and the like.

2. Overview of the model

As illustrated in fig. 1, the sodium currents are calculated as the product (mathematical convolution) of a normalized Gaussian distribution of opening times, a normalized mathematical description of the kinetics for a consecutive reaction,

$$\underset{\text{closed}}{\text{A}} \xrightarrow{k_1} \underset{\text{conducting}}{\text{C}} \xrightarrow{k_2} \underset{\text{closed}}{\text{D}} ,$$

and a current factor which scales the product curve to the measured current. The Gaussian distribution was chosen to approximate the true distribution and to make the mathematics expressible in a closed-form equation.

As was demonstrated previously, the distribution of opening times is consistent with an origin

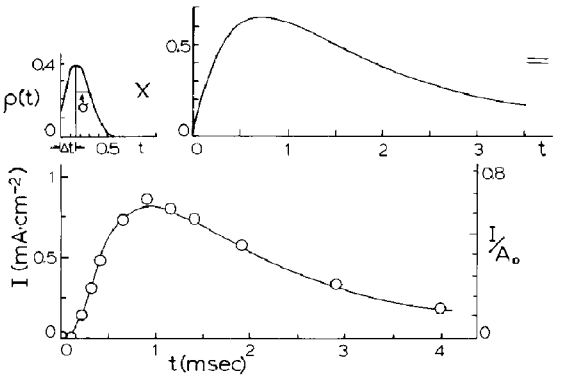

Fig. 1. The components of the nonhomogeneous kinetic model for the voltage clamp currents. (Top left) The opening times of the collection of channels are distributed in a Gaussian distribution characterized by a delay time to the peak of Δt and a width in time, σ. This is multiplied by the fraction of channels open over time (top right) to yield the kinetics of the channels. The resulting curve is multiplied by A_0 to fit the measured current (bottom). The data shown here are for the 50 mV depolarization of the nerve before pentane was added ('A'). The fit illustrated is typical of those in this set. The values of the variables are given in table 1.

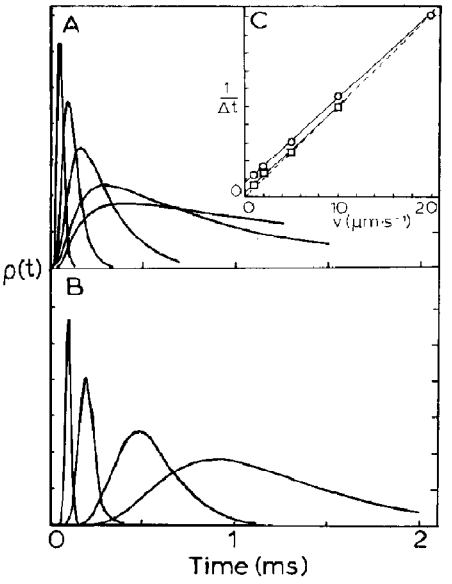

Fig. 2. The nature of the Gaussian time distribution approximation. Graphs A and B show simulations of the distribution of transit times plotted as an arbitrary linear population vs. time. The curve shapes are sensitively dependent on the diffusion coefficient. A plot of $1/\Delta t$ found vs. the velocity is shown in C. Circles are from A, and squares from B. The dotted line in C shows the result expected in the limit of relatively slow diffusion – a Gaussian (symmetrical) peak appears. There is certainly some error associated with the use of a normalized Gaussian distribution in time. However, the mathematical and computational simplicity argues for its use. The number density distributions shown in A and B are found as follows. The reactable species is assumed to be at distance $x = 0$ at $t = 0$ in a delta-function distribution. It becomes reactable as it reaches a distance $\bar{d}$ away. The resulting distribution in time is calculated from the equation

$$\rho(t) = M/\left[2(\pi Dt)^{1/2}\right] \exp\left[-(\bar{d} - vt)^2/4Dt\right]$$

where M scales the distribution, D is the diffusion constant, and v the ion velocity. A constant value of $\bar{d}$ is assumed equal to 10 Å. Note the diffusion coefficient is 10-times larger for A than B. (A) $D = 1\times10^{-11}$ cm^2 s^{-1}; v (sharp to broad) are 2×10^{-3}, 1×10^{-3}, 5×10^{-4}, 2×10^{-4}, 1×10^{-4} cm s^{-1}. (B) $D = 1\times10^{-12}$ cm^2 s^{-1}; v (sharp to broad) are 1×10^{-3}, 5×10^{-4}, 2×10^{-4}, 1×10^{-4} cm s^{-1}.

in simultaneous electrodiffusion * and thermal diffusion processes. The characteristics of the Gaussian approximation are illustrated in fig. 2. The time distribution is a continuum.

It should be understood that the distribution reflects an integral part of the kinetics. One might write the stoichiometric equation including the diffusional term in the following manner.

$$\text{(distributed continuum form)} \overset{\text{diffusional}}{\rightarrow} A \overset{k_1}{\rightarrow} C \overset{k_2}{\rightarrow} D$$

However, with good reason, this type of expression has not been used to describe numerous chemical processes which involve both mass transport and Arrhenius-type rates: e.g., electrode kinetics [17,18] and radiation-induced reactions [12]. One problem with this nomenclature is that it does not suggest the random transformations within the distributed forms nor the possibility of transitions from or to a number of different forms from an observable single state (such as A).

Finally, one can consider the period of the presence of the conducting form, C, as a time window. The behavior within this time allows

* A significantly different model utilizing electrodiffusive processes was created by Neumcke et al. [14]. A review of earlier considerations of electrodiffusion related to squid nerve appeared in 1965 [16].

inferences to be made about the preceding and following states of the system. However, firm conclusions require more direct measurements of all the molecular states. Thus, the exact natures of states A and D are still open to wide surmise.

With the present kinetic model, the following variables are used to fit the current-time curves: Δt, the delay time to the midpoint of the distribution of times; σ, the standard deviation of the width of the distribution; k_1, the on rate constant; k_2, the rate constant for the decay upon prolonged depolarization; A_0, the scaling term for the current. From previous work [5,7] these variables in the equation describing the currents are found to possess the characteristic behaviors illustrated in fig. 3. The following characteristics of the graphs (fig. 3a–f) should be noted.

(a) A plot of $1/\Delta t$ vs. potential is a straight line. The extrapolation of this line intersects the baseline at a potential V_s from the holding potential.

(b) A plot of σ vs. $\Delta t^{3/2}$ is a straight line. The extrapolation of this line towards the origin passes near to the origin.

(c) A plot of log k_1 vs. potential is a straight line.

(d) A plot of k_2 vs. potential has exhibited two types of behavior. One shows a horizontal straight line: k_2 is approximately constant. The other consists of a linear decrease followed by a linear increase with the minimum near the zero of transmembrane potential.

(e) A plot of A_0 vs. potential shows a rising phase and a linear falling phase.

(f) A plot of the ratio of the measured value of A_0 (the dots in fig. 3e) to its expected value (dashed line in fig. 3e) vs. potential yields a curve with a rising portion reaching a plateau. This ratio was called f in the earlier papers. From single-channel measurements, it is now clearly the probability of a channel being open, which is usually designated by P or P_{open}. The data found from noise measurements and as derived here from voltage-clamping are directly comparable.

The values of the variables as determined from fitting of Haydon and Kimura's voltage-clamp data [20] are listed in table 1.

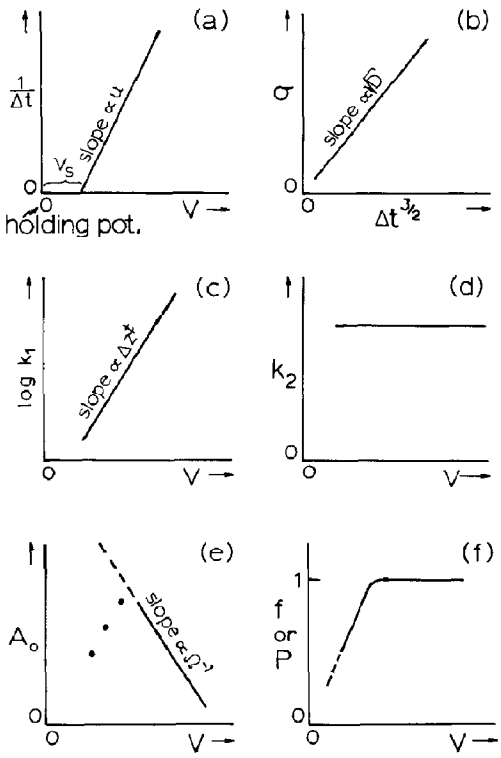

Fig. 3. Graphs illustrating the behaviors of the variables of the nonhomogeneous model found when fitting experimental currents. (a) The straight line resulting from plotting $1/\Delta t$ vs. the depolarization potential is characterized by a slope proportional to an ion mobility over a fixed distance. The extrapolated V-intercept is at the point of the intramembrane zero potential. V_s is the shielding potential. (b) The straight line resulting from plotting σ vs. $\Delta t^{3/2}$ is characterized by the square root of a diffusion coefficient. (c) The straight line resulting from plotting log k_1 vs. the depolarization potential is characterizable by a single charge of activation. (d) The value of k_2 is essentially independent of potential. (e) A plot of A_0 vs. the transmembrane potential has a linear segment with a slope proportional to the conductance. (f) A plot of the proportion of channels open shows a sigmoid shape reaching saturation. Two parameters characterize it: a potential where $P = 0.5$ and a parameter describing the sharpness of the sigmoidal curve.

3. Support for the model

A number of characteristics and predictions of the author's model have been confirmed. Among these are:

The existence of the last step in a channel's

Table 1

Variable values found from curve fitting

Experimental conditions [20]: external medium (mM) – 215 NaCl, 215 choline Cl, 10 KCl, 10 $CaCl_2$, 50 $MgCl_2$, 10 Trisma (pH 7.6); internal medium (mM) – 340 CsF, 400 sucrose, 10 NaCl, 10 Hepes (pH 7.3). Holding potential, −70 mV. Prepulse protocol; holding potential/−90 mV (50 ms)/depolarization. Temperature (°C), 7±1. *n*-Pentane concentration, 275 μM.

Depolarization (mV)	k_1 (s^{-1})	k_2 (s^{-1})	Δt (μs)	σ (μs)	A_0 (mA cm^{-2})
Standard ('A')					
30	1108	709	436	239	1.333
40	1890	700	250	157	1.921
50	2667	595	186	108	2.520
60	4140	574	139	34	2.407
70	5228	656	131	39	2.203
80	6561	705	124	30	1.834
90	9237	708	138	32	1.419
+ Pentane ('B')					
30	2136	953	262	120	1.348
40	3189	988	197	105	1.751
50	5269	818	101	48	1.435
60	7279	896	115	32	1.254
70	10838	957	106	29	1.051
80	14744	1010	117	30	0.881
90	13501	995	97	10	0.644
Pentane removed ('C')					
30	1000	735	800	419	0.452
40	1380	652	419	250	1.243
50	1970	599	252	84	1.853
60	2816	603	199	69	2.133
70	4368	543	157	45	1.808
80	6474	422	147	8	1.424
90	8789	483	157	6	1.198

opening – characterized by k_1 – caused by an approximately monovalent charge transfer [21] across an interface.

The probability of a channel being open changes with potential. Low at small depolarizations [4,21,22], it reaches an upper limit around −10 mV transmembrane potential. This result is derived from A_0 and described by P_{open}.

The slow inactivation upon prolonged depolarization, characterized by k_2, may be voltage-independent [4,23,24]. However, some voltage-dependent effects also have been seen (ref. 25 and this work).

The charge of activation involved with the rapid repolarization is found to be equal to that for the final channel-opening step as expected from the usual behavior [26] of such processes (but see ref. 27).

In addition, the model is in agreement with the observation by Fishman et al. [28] that the sodium channel noise spectrum indicates that a nonreversible process is involved.

4. Physical interpretation

A physical interpretation of the events leading to the observed currents follows from the relatively simple behavior of the variables and known descriptive chemistry.

4.1. From Δt and σ

Net ionic velocities are zero in the absence of an electric field. In the nerve, the peak of the distribution of transit times behaves as expected

for an electrodiffusion. Therefore, the linear extrapolation of the ionic velocity to zero – $1/\Delta t = 0$ – indicates the true intramembrane zero potential at the region of the motion. The intramembrane zero potential does not occur at the holding potential as seen in figs. 3a and 5. The difference between the holding potential and the $1/\Delta t$ intercept is the voltage equivalent of the shielding – V_s. The following conclusion is suggested.

(1) At the site of molecular action, the potential jump is partly shielded – most likely from changing surface charges. (This effect was expected by Cole [16] and also discussed in some detail in Haydon et al. [20,29] for alkane-treated squid nerves.)

In the case of the sodium channel, the cause of the distribution of opening times may be viewed as the motion of a sheet of charges. As illustrated in fig. 4, the plane of the center-of-charge of the sheet moves under the influence of the external

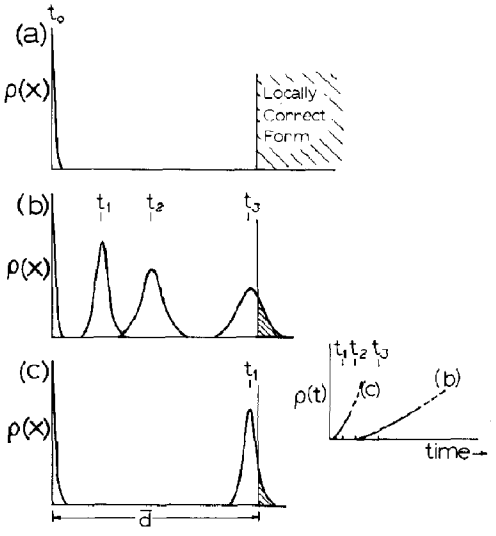

Fig. 4. Visualizing the charge movement associated with the delay time and its distribution. (a) The charged material is held in a narrow distribution at a distance $\bar{d}$ from a conformation where the channel opening step – k_1 – can proceed. (b) After a depolarization, the charged material migrates and its distribution broadens. The shaded fraction possesses the correct conformation. (c) The same as (b) but with a larger depolarization so that the migration is faster and less time exists for diffusional broadening. At the right is illustrated the effects observed in the time domain for the two figures.

field – electrodiffusion – while the charge distribution in the sheet simultaneously broadens due to Brownian motion. These motions are related to the slopes of graphs of the types shown in fig. 3a and b. The slope of fig. 3a is characteristic of electrodiffusion; the slope of fig. 3b is characteristic of Brownian motion in the moving frame of reference. Therefore, the following conclusion is suggested.

(2) Upon depolarization, the initial ionic motion is diffusive. Both electrodiffusion and Brownian diffusion occur simultaneously (both quasi-diffusion). The process occurs inside the membrane. The description is equivalent to motion described by the Fokker-Planck equation [30,31] although the explicit form of the differential equation is not used.

A directly measured diffusion coefficient of the sodium channel [32] agrees closely with the diffusion coefficient calculated from the model (ref. 5 and this work). Both are in the range for general protein diffusion in membranes [19]. Because a one-dimensional diffusion involves atomic jumps in directions perpendicular to the measured direction of travel, both transverse and lateral diffusion coefficients (for the quasi-diffusion) are expected to be of the same order of magnitude. The following conclusion is suggested.

(3) The diffusing species is a relatively large fraction of the entire sodium channel. The diffusion may be transverse or lateral. The matrix through which the quasi-diffusion proceeds may be the membrane, the protein assembly, or a combination of both membrane and protein.

Since the measurements of the electrodiffusion and the thermal diffusion are made simultaneously, we find that:

(4) The magnitude of the net charge which diffuses can be determined from the data. When assuming a dielectric coefficient of unity and assuming the charge transverses the full applied potential, the net charge moving has been found to be in the range of 3–15 elementary charges depending on the conditions.

4.2. From k_1

The logarithmic dependence of k_1 on voltage is characterizable by a charge of activation, $\Delta z^{\ddagger}$

[26]. Conclusions 5 and 6 follow from this.

(5) After the initial diffusive motion, the next reaction step is characteristic of charging (or discharging) at an interface. The charge of activation is in the range of unity. This is a reversible (as opposed to a dissipative) reaction. Possible mechanisms for such behavior might be the filling or emptying of an ion site in the channel with an ion that crosses the solution/membrane interface.

(6) The reversal of step 5 occurs when the external potential jump is reversed. This rapid channel turnoff is characterized by the same charge of activation. This process is commonly characterized by Hodgkin and Huxley's β_m.

4.3. From k_2

Conclusion 7 follows from the constancy of k_2. (When k_2 does appear to be voltage-dependent, its relative change is small compared to that shown by k_1 or Δt.)

(7) The slow turnoff upon prolonged depolarization (Hodgkin and Huxley's h-process) may be a voltage-independent reaction. Voltage independence is consistent with a number of different physical processes: (a) Charge motion perpendicular to the applied field; (b) the motion of neutral – e.g., ion paired – species; (c) a restoring force provided by protein chains of the channel acting as rubber-like springs. This last suggestion is supported by evidence described in the following paper [15a].

4.4. From A_0

The voltage dependence of A_0 exhibits a rise followed by a linear downward-sloping segment. A straightforward analysis of the potential dependence of the A_0 curve yields the same results as found from multiple pulse experiments,

(8) The extrapolation (if necessary) of the linear segment intersects the zero-current axis at the sodium transmembrane potential.

The interpretation of the underlying molecular processes leading to the voltage dependence of P is the topic of the following paper. However,

(9) The P value reflects a quasi-equilibrium of the sodium channel which is stable over the millisecond time course of the experiments.

5. Results of the analysis: the effects of *n*-pentane

The data for the analysis were obtained from published data [20]. Approx. 15 current-time points were used for each curve with the number concentrated at the early times through the peak. An example of a typical fit is illustrated in fig. 1. No correction for leakage was able to be made since the information needed was unobtainable. The precision of the numerical data was such that the uncompensated leakage produced by far the greatest error. This error produces the largest effect in values of k_2.

The numerical values of the variables for the curves at each depolarization potential are found by using a non-linear least-squares fit of the data. The fitting program – which is the same one previously run on a mainframe system [5] – was translated into BASIC and run on a personal computer which operates with 16-bit precision for mathematical calculations (Commodore 8032). The values of the variables found here from the experimental currents are listed in table 1.

Graphical presentations of the variables found from data fitting are shown in figs. 5–10. The parameters characterizing the variables found from the data fitting are summarized in table 2. It should be noted in passing that because straight-line relationships are expected in the plots, random errors from the data can be averaged. As an extra benefit, deviations are easily seen and standard deviations can be calculated.

The slopes and/or intercepts of the best-fit lines of each of the six types of graph are characterized by parameter values. These are

Fig. 5: V_s and the slope $d(1/\Delta t)/dV$ for $1/\Delta t$ vs. the depolarization voltage.

Fig. 6: D (using an assumed average distance) for σ vs. $\Delta t^{3/2}$

Fig. 7: $\Delta z^{\ddagger}$ for log k_1 vs. the depolarization voltage.

Fig. 8: $\langle k_2 \rangle$ for k_2 vs. depolarization voltage.

Fig. 9: a conductance for the linear portion of

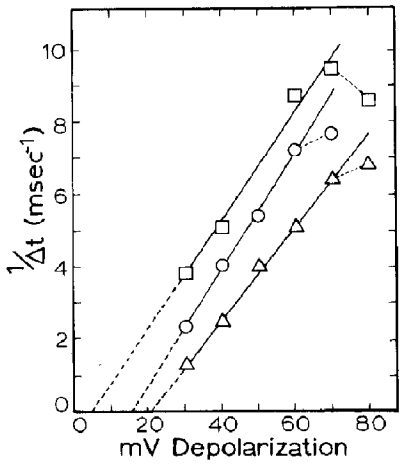

Fig. 5. A plot of $1/\Delta t$ vs. depolarization voltage for the three sets of data. (○) The standard ('A'), (□) with pentane present ('B'), (△) after recovery ('C'). The letters refer to the entries in table 1. Parameter values for the curves are listed in table 2. The experimental conditions are listed in table 3. The straight lines are least-squares fits to the data.

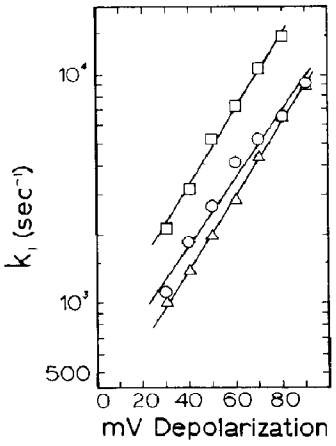

Fig. 7. Plot of log k_1 vs. depolarization voltage for the three sets of data. (○) The standard ('A'), (□) with pentane present ('B'), (△) after recovery ('C'). The straight lines are least-squares fits to the data. The slopes are equivalent to a decadic change in (A) 68 mV, (B) 59 mV and (C) 62 mV.

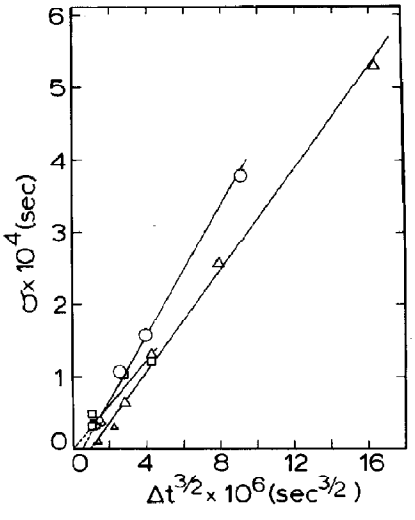

Fig. 6. Plot of σ vs. $\Delta t^{3/2}$ for the three sets of data. The larger values are from the smaller depolarizations. (○) The standard ('A'), (□) with pentane present ('B'), (△) after recovery ('C'). The straight lines are least-squares fits to the data. The fitting equations are: (A) $46.8\Delta t^{3/2} - 3.0\times10^{-5}$; (B) $31.9\Delta t^{3/2} - 4.3\times10^{-6}$; (C) $34.9\Delta t^{3/2} - 3.2\times10^{-5}$.

A_0 vs. V and a value for V_{Na} assuming a linear extrapolation to $A_0 = 0$.

Fig. 10: shown are two of possibly many different ways to characterize P vs. V. These two are discussed briefly below and in more detail in the following paper.

As can be seen from figs. 5–10 and table 2, the following properties are left unchanged by the presence or absence of *n*-pentane:

(a) V_{Na}, the sodium transmembrane potential

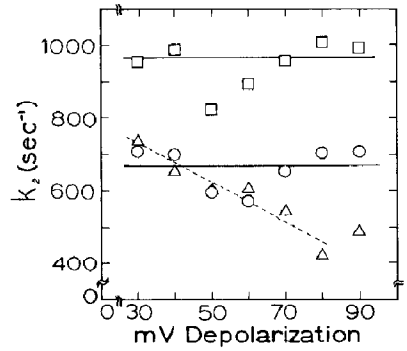

Fig. 8. Plot of k_2 vs. depolarization voltage for the three sets of data. (○) The standard ('A'), (□) with pentane present ('B'), (△) after recovery ('C'). The straight lines are least-squares fits to the data.

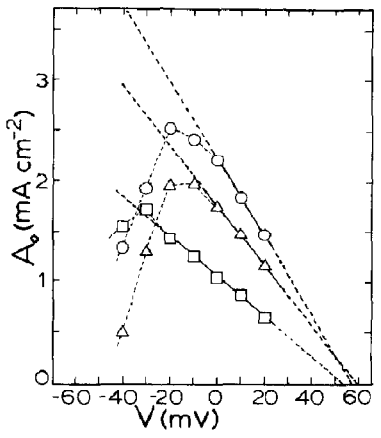

Fig. 9. Plot of A_0 vs. transmembrane potential voltage for the three sets of data. (○) The standard ('A'), (□) with pentane present ('B'), (△) after recovery ('C'). The straight lines are least-squares fits to the data on the solid line.

(table 2, line 7). The values agree within 6 mV.

(b) $\Delta z^{\ddagger}$, the net charge of activation for the last step of activation (the process characterized by k_1) (table 2, line 1). The lines plotted in fig. 7 are essentially parallel.

(c) The intramembrane ionic velocity – specifically of the entity/entities responsible for the electrodiffusion effects (table 2, line 3). The slopes of the lines in fig. 5 are nearly parallel and without correlation with the presence of pentane.

The observed changes in the voltage-clamp currents can be explained by changes in three properties of the nerve. These are:

Table 2

Table of numerical results from data fitting [a]

Line number	A (Standard)	B (+275 μM pentane)	C (after recovery)
From log k_1 plots (fig. 9):			
(1) $\Delta z^{\ddagger}$ (at 6°C)	0.8_2	0.9_4	0.90
From $1/\Delta t$ plots (fig. 5):			
(2) V_s	$15._6$ mV	$4._6$ mV	$20._5$ mV
(3) $d(1/\Delta t)/d\Delta V$ (ion mobility)$^{-1}$	1.6×10^5 V^{-1} s^{-1}	1.5×10^5	1.3×10^5
From k_2 plots (fig. 8):			
(4) $\langle k_2 \rangle$	$6._7\times10^2$ s^{-1}	$9._7\times10^2$ s^{-1}	–
From σ vs. $\Delta t^{3/2}$ plots (fig. 6):			
(5) D for $\bar{d}=10$ Å	4.4×10^{-11} cm^2 s	$1._8\times10^{-11}$	2.4×10^{-11}
From A_0 plots (fig. 9):			
(6) conductance, g'_{Na}	39 mS cm^{-2}	$19._5$	29.3
(7) V_{Na} (linear extrapolation)	+56 mV	+54 mV	+60 mV
From σ vs. $\Delta t^{3/2}$ and $1/\Delta t$ plots (figs. 5 and 6):			
(8) z (constant $\bar{d}$, full ΔV, $\epsilon=1$)	3.5	8 ± 2	$5._1$
From plots of P (fig. 10):			
Nernst analysis			
(9) $V_{P=0.5}$	−34 mV	–	−30 mV
(10) net charges	$-2._6$		−3.8
Complementary error function			
(11) $V_{P=0.5}$	−33 mV	–	−30 mV
(12) Factor in erfc[factor·$(V-V_{1/2})$] (V in volts)	44.5		70.9
Shift in true internal zero potential relative to standard:			
(13) From log k_1 at $k_1=800$	0 (std)	−12 mV	+9 mV
(14) From $1/\Delta t$ extrapolation	0 (std)	−11 mV	+5 mV
(15) From plots of P	0 (std)	−15 mV [b]	+4 mV [c]

[a] Estimated errors are approximately one unit in last digit or five in subscript digits (from statistics of linear fit of parameters).
[b] One point only.
[c] At mid-point ($P=0.5$).

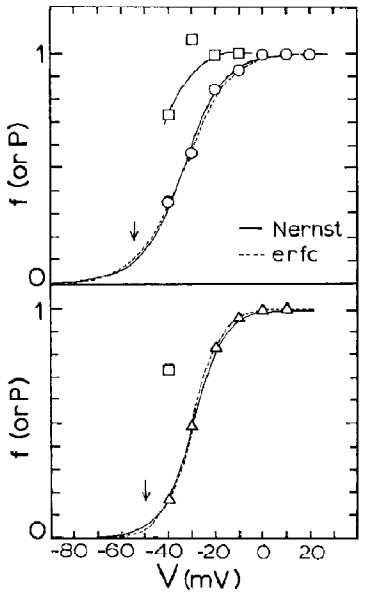

Fig. 10. Plot of P vs. transmembrane potential voltage for the three sets of data. (○) The standard ('A'), (□) with pentane present ('B'), (△) after recovery ('C'). The solid lines are least-squares fits to the data with the equation $P = [\exp Q/(1 + \exp Q)]$ where $Q = -[z(V - V_{P-0.5})/0.024]$ at 6°C. The dashed line is fitted by $P = \text{erfc}[\text{factor} \cdot (V - V_{P-0.5})]$ with V in volts.

(1) A shift in shielding of the intramembrane region from the external field (table 2, lines 13–15 derived from lines 2 and 9 or 11). This is seen in three different parameter plots: those for $1/\Delta t$, k_1, and P (figs. 5, 7 and 10) vs. voltage. The results from all three agree within the experimental and calculational errors.

(2) Lowering of the Na conductance in the presence of n-pentane (table 2, line 6). As noted by Haydon and Kimura, only partial recovery is seen. This effect is seen in the slopes of the straight line segments of fig. 9.

(3) Acceleration of the slow turnoff (k_2 increases) in the presence of n-pentane (table 2, line 4).

Since the values for σ are less sensitive to the data fit, the value of D characterizing them is less certain. It is not clear whether there is:

(4) A possible decrease in diffusion coefficient, D, of the body/bodies in the membrane (table 2, line 5).

One cause of the changes seen upon applying pentane may be:

(5) An increase of the net charge on the moving body/bodies in the membrane (table 2, line 8) in the presence of pentane. Again, this conclusion is less certain due to the relatively large scatter of the σ values.

Finally, the sigmoidal graph of P vs. potential is sharper after the partial recovery from the pentane perturbation (table 2, lines 10 and 12). This reflects changes in the quasi-equilibrium state of the channels.

6. Discussion

This section is divided into two parts. First, the conclusions of Haydon and Kimura's analysis are compared with the results of this analysis. Second, some possible molecular properties of the channel which can be inferred from the data and this model are presented.

6.1. Descriptive parameters

Within the formalism used here, the changes in sodium currents can be explained somewhat more simply than done using the Hodgkin-Huxley model as done by Haydon and Kimura [20]. With regard to the kinetics: both of the models indicate a change in the channel turnoff rate. And both suggest a shift in the intramembrane voltage shielding. On the one hand, Haydon suggests that the turn-on rate constant changes depending on conditions. However, the results from the rate analysis here demonstrate that these changes are due to the shielding alone: the linear plots of $\log k_1$ and $1/\Delta t$ are shifted equally.

It should be noted that the values of k_2 are not as constant here as they appear for other data analyzed in an earlier paper [5]. Among the reasons may be the lack of resistance compensation and/or the leakage of the membrane. One expects to need the greatest resistance compensation with the largest currents. The values of k_2 seem to be inversely dependent on the magnitude of the in-

ward current indicating a possible dependence on this factor.

The conductance of the clamped area of the membrane decreases with the application of *n*-pentane and partially recovers upon returning the nerve to its original solution. Both formalisms indicate this point.

The quasi-equilibrium P value is the probability that a channel is open, and is directly comparable to the same quantity found from single-channel measurements. As seen from table 2, lines 13–15, the P value curves are shifted due to shielding by the same amount as found from the kinetics. This is an independent measure of the shift since A_0 is independent of the form of (normalized) kinetics.

The voltage and conductance shifts are such that the full P curve is not obtainable from the *n*-pentane-treated nerve. However, the partially recovered membrane indicates that the curve may be sharper in the presence of pentane. There are two different functions used to fit the curves: the Nernstian form and a complementary error function which is the integral of a Gaussian curve. The Nernstian function is the same, in effect, as that used by Hodgkin and Huxley to fit the h_∞ curves and were used by Haydon and Kimura [20] in their fig. 4. The sharpening of the curve implies an increase in the charge in the presence of pentane. This point is discussed below.

6.2. *Information of underlying processes*

In addition to the descriptive variables, the changes in their associated parameters suggest possible underlying causes for the action of pentane. For instance, $\Delta z^\ddagger$ – the charge of activation for the k_1 process – can be interpreted as a less-than-unit net charge associated with the rate-controlling step. On the other hand, if we assume that the charge is 1.00, the value then becomes the fraction of the transmembrane potential traversed. This is in the range of 80–95% and is in agreement with previous work [5]. * It appears that the value of $\Delta z^\ddagger$ remains unchanged in the presence of *n*-pentane. (The values are the same within a standard deviation.) Since V_{Na} also remains unchanged, it appears that the presence of pentane has no effect on processes that occur within the solution environment. However, the similar shifts in potential of the plots of log k_1, $1/\Delta t$ and P_{open} indicate that the potential inside the membrane does change with pentane.

The parameter values indicate that while the ionic mobility changes only slightly if at all, there is a decrease in the diffusion constant when pentane is present. For the usual classical viewpoint, the diffusion constant decreases because of an increase in viscosity and/or an increase in size. (Of the two properties, we usually expect that the viscosity can be changed by relatively large amounts more easily.) If the viscosity increases, we expect that, ceteris paribus, the ion mobility will decrease **. However, it appears that there is an approximately compensating increase in the charge – $|z|$ (table 2, line 8) – which keeps the ion mobility constant.

The calculated value of $|z|$ is not independent of other, associated variables. Nevertheless, it does change in tandem with the steepness of the P_{open} vs. voltage plot, which is not dependent on the kinetics. (The Nernstian charge and the factor in the complementary error function used to fit the P_{open} curve (table 2, line 10 or 12) reflect the steepness.) Whether this charge-viscosity compensation is adventitious or causally related is still an open question.

7. The sodium channel as a probe of polymer motion

As opposed to most man-made polymers, the sodium channel as a protein is expected to be nearly monodisperse. In addition, the channels are oriented – fixed in the membrane and oriented relative to the applied electric field. The currents appearing while a channel is in the conducting

* The number $\Delta z^\ddagger$ was incorrectly given as 1.13 in ref. 5, p. 256, and should have been 0.88.

** Related to the ion velocity, there is an error in ref. 5 in the last equation of the left column on p. 252. It should be v/force. The conclusions remain unchanged. However, the surrounding material is less viscous than noted.

(open) state offer a powerful probe of the presence of one specific channel conformation. This unique combination of properties may be useful in probing fundamental questions of macromolecular conformation and relaxation. In addition, the variations in the apparent shielding of the applied voltage – as seen in the wide variations of V_s under different conditions – would appear to offer a sensitive probe of the solution/membrane interfaces near the channel sites.

Appendix: Determining the charge on the diffusing species

The fundamental equation (eq. A1) relates the diffusion coefficient, D, to the velocity, v, due to the force, F, on a particle.

$$\frac{kT}{D} = \frac{F}{v} \tag{A1}$$

In the equation, k is the Boltzmann constant and T the absolute temperature. A clear discussion of this equation appears in a review by Barker [33].

It is common to separate the processes of electrodiffusion and thermal diffusion through an approximate model of the motion: a sphere of radius r passing through a homogeneous fluid with viscosity η. As a result, the term $6\pi\eta r$ appears and yields the Stokes equation, eq. A2, and the Einstein-Stokes equation, eq. A3.

$$v = \frac{F}{6\pi\eta r} \tag{A2}$$

$$D = \frac{kT}{6\pi\eta r} \tag{A3}$$

In measuring the distribution of firing times of the sodium channels in the clamp, both the thermal diffusion and electrodiffusion of the same entity (or entities) are quantified simultaneously. As a result, its net charge can be determined in the manner derived below.

The force on a particle with $|z|$ charges in an electric field is given by

$$F = 1.602 \times 10^{-12} |z| \text{ dyn V}^{-1}\text{ cm} \tag{A4}$$

In other words, for an electric field of 1 V cm^{-1}, the force on a particle with unit elementary charge is $F = 1.602 \times 10^{-12}$ dyn.

The field, which is generated over the distance the charged species moves, is related to the applied voltage by

$$E(\text{V cm}^{-1}) = \frac{V_{\text{eff}} \cdot \phi}{\bar{d}\epsilon} \tag{A5}$$

where V_{eff} is the potential across the membrane having taking the shielding V_s into account; $\bar{d}$ the distance over which the charged species moves; ϕ the fraction of the applied potential which appears across that distance; and ϵ the effective dielectric constant. Note that $0 \leqslant \phi \leqslant 1$.

As a result, the force appearing in eq. A1 can be written as

$$F = 1.602 \times 10^{-12} |z| \frac{V_{\text{eff}} \cdot \phi}{\bar{d}} \tag{A6}$$

The velocity of the molecular species is simply related to Δt by

$$\bar{d} = v\Delta t$$

or

$$v = \bar{d}(1/\Delta t) \tag{A7}$$

Label the slope of the σ vs. $(\Delta t)^{3/2}$ graph with the Greek letter β. From the model [2],

$$\beta = \sqrt{2D}/\bar{d}$$

Thus,

$$D = \tfrac{1}{2}\beta^2\bar{d}^2 \tag{A8}$$

and eq. A1 may be rewritten.

$$\frac{2kT}{\beta^2\bar{d}^2} = \frac{1.60 \times 10^{-12}|z|}{\bar{d}^2} \cdot \frac{\phi}{\epsilon} \cdot \frac{V_{\text{eff}}}{(1/\Delta t)} \tag{A9}$$

Cancelling out the average-distance terms and rearranging, eq. A9 becomes

$$|z| = \frac{kT}{1.60 \times 10^{-12}} \cdot \frac{\epsilon}{\phi} \cdot \frac{(1/\Delta t)}{V_{\text{eff}}} \cdot \frac{1}{\beta^2} \tag{A10}$$

For $T = 280$ K, eq. A10 yields

$$|z| = 0.043 \frac{\epsilon}{\phi} \cdot \frac{(1/\Delta t)}{V_{\text{eff}}} \cdot \frac{1}{\beta^2} \tag{A11}$$

The term

$$\frac{(1/\Delta t)}{V_{\text{eff}}}$$

is a constant and equals the slope of the plots of $1/\Delta t$ vs. the depolarization voltage. Thus, the value of $|z|\phi/\epsilon$ is fixed unambiguously by the parameters describing the experimental results. In reporting the values of $|z|$ found, it is assumed that $\epsilon = 1$ and that the entire potential is traversed, i.e., $\phi = 1$. Since

$0 \leq \phi \leq 1$ and $\epsilon \geq 1$,

the reported values of $|z|$ are minimum values for the true net charge.

Acknowledgements

I wish to thank Professor Richard Keynes for a useful communication and Richard Horn for important comments.

References

1 R. Horn, J. Patlak and F. Stevens, Nature 291 (1981) 426.
2 R. Horn, C.A. Vandenberg and K. Lange, Biophys. J. 45 (1984) 323.
3 R. Ten Eick, J. Yeh and N. Matsuki, Biophys. J. 45 (1984) 70.
4 R.W. Aldrich, D.P. Corey and C.F. Stevens, Nature 306 (1983) 436.
5 K.A. Rubinson, Biophys. Chem. 15 (1982) 245.
6 N.J.B. Green, M.J. Pilling, P. Clifford and W.G. Burns, J. Chem. Soc. Faraday Trans. 1, 80 (1984) 1313 and references therein.
7 K.A. Rubinson, J. Physiol. 281 (1978) 14P.
8 E.W. Knapp, S.F. Fischer and F. Parak, J. Phys. Chem. 86 (1982) 5042.
9 N. MacDonald, Time lags in biological media (Springer-Verlag, Berlin, 1978).
10 A. Peterlin, J. Polym. Sci. Polymer Symposia 43 (1973) 187.
11 R.I. Cukier and K. Lakatos-Lindenberg, J. Chem. Phys. 57 (1972) 3427.
12 F. Heatley and A. Begum, Polymer 17 (1976) 399.
13 R. Horn and C.A. Vandenberg, J. Gen. Physiol. 84 (1984) 505.
14 B. Neumcke, W. Nonner, and R. Stampfli, in: International Review of Biochemistry, ed. J.C. Metcalfe (University Park Press, Baltimore, 1978) vol. 19, ch. 5, p. 129.
15 H. Fishman, Prog. Biophys. Mol. Biol. 46 (1985) 127.
a. K.A. Rubinson, Biophys. Chem. 25 (1986) 57.
16 K.S. Cole, Physiol. Rev. 45 (1965) 340.
17 P. Delahay, J. Am. Chem. Soc. 74 (1952) 1430.
18 A.J. Bard and L.R. Faulkner, Electrochemical methods (Wiley, New York, 1980) ch. 3.
19 R.J. Cherry, Biochim. Biophys. Acta 559 (1979) 289.
20 D.A. Haydon and J. Kimura, J. Physiol. 312 (1981) 57.
21 T. Begenisich and D. Busath, J. Gen. Physiol. 77 (1981) 489.
22 H.M. Fishman, H.R. Leuchtag and D. Poussart, Biophys. J. 45 (1984) 46.
23 C.M. Armstrong and F. Bezanilla, J. Gen. Physiol. 70 (1977) 567.
24 W. Nonner, J. Physiol. 299 (1980) 573.
25 R.P. Swenson, Jr, Biophys. J. 41 (1983) 245.
26 K.A. Rubinson, Biophys. Chem. 12 (1980) 51.
27 L.-Y.M. Huang, N. Moran and G. Ehrenstein, Biophys. J. 45 (1984) 313.
28 H.M. Fishman, H.R. Leuchtag and L.E. Moore, Biophys. J. 43 (1983) 293.
29 D.A. Haydon, B.M. Hendry, S.R. Levinson and J. Requena, Biochim. Biophys. Acta 470 (1977) 17.
30 S. Chandrasekhar, Rev. Mod. Phys. 15 (1943) 1.
31 D.K.C. MacDonald, Noise and fluctuations: an introduction (Wiley, New York, 1962) p. 70ff and especially fig. 16.
32 W. Almers, P.R. Stanfield and W. Stuhmer, J. Physiol. 336 (1983) 261.
33 R.E. Barker, Jr, Pure Appl. Chem. 46 (1976) 157.